LETTER

doi:10.1038/nature14278

Saturn's fast spin determined from its gravitational field and oblateness

Ravit Helled[1], Eli Galanti[2] & Yohai Kaspi[2]

The alignment of Saturn's magnetic pole with its rotation axis precludes the use of magnetic field measurements to determine its rotation period[1]. The period was previously determined from radio measurements by the Voyager spacecraft to be 10 h 39 min 22.4 s (ref. 2). When the Cassini spacecraft measured a period of 10 h 47 min 6 s, which was additionally found to change between sequential measurements[3,4,5], it became clear that the radio period could not be used to determine the bulk planetary rotation period. Estimates based upon Saturn's measured wind fields have increased the uncertainty even more, giving numbers smaller than the Voyager rotation period, and at present Saturn's rotation period is thought to be between 10 h 32 min and 10 h 47 min, which is unsatisfactory for such a fundamental property. Here we report a period of 10 h 32 min 45 s ± 46 s, based upon an optimization approach using Saturn's measured gravitational field and limits on the observed shape and possible internal density profiles. Moreover, even when solely using the constraints from its gravitational field, the rotation period can be inferred with a precision of several minutes. To validate our method, we applied the same procedure to Jupiter and correctly recovered its well-known rotation period.

Previous theoretical attempts to infer Saturn's rotation period have relied on wind observations derived from cloud tracking at the observed cloud level[6]. One theoretical approach was based on minimizing the 100 mbar dynamical heights[7] with respect to Saturn's measured shape[8], while a second approach was based on analysing the potential vorticity in Saturn's atmosphere from its measured wind profile[9]. The derived rotation periods were found to be 10 h 32 min 35 s ± 13 s, and 10 h 34 min 13 s ± 20 s, respectively. Our optimization method is based on linking the rotation period of Saturn with its observed physical properties and their uncertainties, in particular, the gravitational field. The method allows us to derive Saturn's rotation period for different types of constraints, and does not rely on a specific interior model, equation of state, wind properties, or other indirect measurements.

The gravitational moments and the internal density profile can be related through the smallness parameter $m = \omega^2 R^3/GM$, where R is the planet's mean radius, M is its mass, G is the gravitational constant, and $\omega = 2\pi/P$ is the angular velocity associated with the rotation period P (refs 10 and 11). The even gravitational moments can be expanded as a function of m by $J_{2n} = \sum_{k=n}^{3} m^k a_{2n,k}$, where $a_{2n,k}$ are coefficients that are determined by the radial density distribution (see Methods). The expansion can go to any order of n; since at present only J_2, J_4 and J_6 are known for Saturn (and Jupiter), in this study we take $n = 1, 2, 3$.

The relation for J_{2n} shows that the measured gravitational moments are determined from the combination of the internal density distribution ($a_{2n,k}$) as well as rotation (m). Our goal is to find a solution for m and $a_{2n,k}$ that minimizes the difference between the observed and calculated J_{2n} within the observed uncertainties. The $a_{2n,k}$ can be expressed by a combination of figure functions (see Methods) that represent a given internal density profile, and can then be linked to the gravitational moments[10,12,13]. However, since in this case there are only three equations and seven unknowns (six figure functions and the smallness parameter), there is no unique solution. As a result, the solution is found by using a statistical optimization approach.

We define an optimization function as the sum of the normalized absolute differences between the observed gravitational moments and the calculated gravitational moments, given by:

$$Y = \sum \left(\frac{\left|J_2 - J_2^{\rm obs}\right|}{\left|\Delta J_2^{\rm obs}\right|} + \frac{\left|J_4 - J_4^{\rm obs}\right|}{\left|\Delta J_4^{\rm obs}\right|} + \frac{\left|J_6 - J_6^{\rm obs}\right|}{\left|\Delta J_6^{\rm obs}\right|} \right) \quad (1)$$

where J_{2n} are the calculated moments, $J_{2n}^{\rm obs}$ are the measured moments, and $\Delta J_{2n}^{\rm obs}$ are the measurement uncertainties of the measured gravitational moments[14,15]. The optimization procedure begins with an initial guess of the various parameters being randomly spread throughout the physical bounds of each parameter. This is repeated 2,000 times to achieve statistical significance. From these 2,000 cases we compute the rotation period and its standard deviation (see Methods). An example of the derived solutions using our optimization method is presented in Fig. 1.

The entire set of solutions for Saturn are summarized in Fig. 2 which shows $P_{\rm calc}$ (dots) and its 1σ standard deviation (blue shading). We first present solutions that are completely unconstrained in radius and density structure, and where the rotation period (grey shading) is allowed to vary widely (Fig. 2a). The fact that the calculated standard deviation is much smaller than the allowed range (blue shading being much narrower than the grey shading) indicates that knowledge of the gravitational

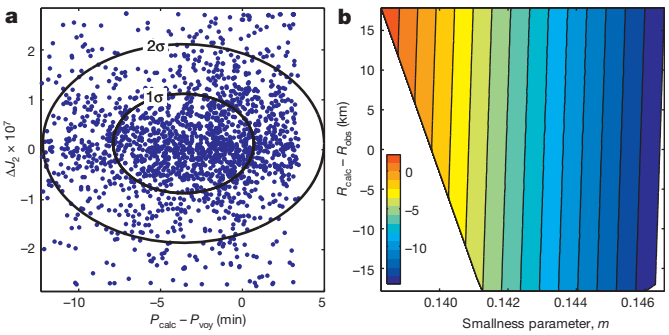

Figure 1 | An example of the statistical distribution of solutions for Saturn's rotation period. For this specific case, the initial possible range of rotation periods is taken to have an uncertainty of 0.5 h around the Voyager radio period (hereafter, $P_{\rm voy}$). The calculated mean radius was set to be within 20 km of Saturn's observed mean radius. The solution is based on an ensemble of 2,000 individual sub-cases, each of them representing a case with specific random initial conditions within the defined parameter space. **a**, A scatter plot of the distribution of solutions on the plane of the calculated rotation period $P_{\rm calc}$ minus $P_{\rm voy}$ = 10 h 39 min 22 s and ΔJ_2. Each blue dot represents one sub-case solution. The inner and outer black circles show the first and second standard deviations, respectively. **b**, The distribution of the derived rotation period with respect to $P_{\rm voy}$ (in minutes) as a function of smallness parameter m and the calculated mean radius $R_{\rm calc}$ minus the observed mean radius of Saturn ($R_{\rm obs}$ = 58, 232 km; ref. 7).

[1]Department of Geosciences, Raymond & Beverly Sackler Faculty of Exact Sciences, Tel Aviv University, Tel Aviv, 69978, Israel. [2]Department of Earth and Planetary Sciences, Weizmann Institute of Science, Rehovot, 76100, Israel.

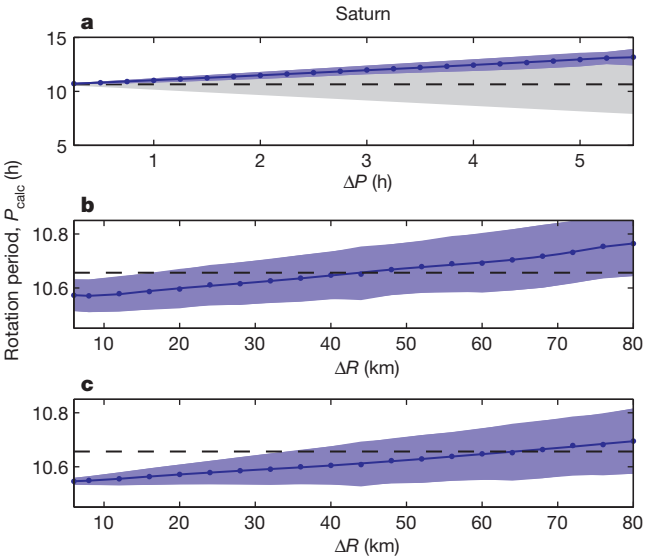

Figure 2 | Solutions for Saturn's rotation period. **a**, The calculated period P_{calc} (blue dots) and its 1σ standard deviation (blue shading) for a large range of cases for which the assumed possible range in rotation period varies between 0.25 h and 5.5 h (grey shading) around P_{voy} (black-dashed line). **b**, P_{calc} and its 1σ standard deviation (blue shading) using $\Delta P = 0.5$ h versus the assumed uncertainty in Saturn's observed mean radius R_{obs}. **c**, As for **b** but when the figure functions are also constrained.

moments can be used to narrow the possible range of rotation periods. In addition, as the initial range of the possible rotation periods is narrower, the derived rotation period can be determined with higher precision. For the smallest range in rotation period (left dot in Fig. 2a) we derive a rotation period of 10 h 43 min 10 s ± 4 min. The fact that the uncertainty in rotation period is decreased without enforcing tight constraints on the model emphasizes the strength of this method. Nonetheless, without any constraints on the shape the solution for the rotation period still has a relatively large range of solutions. In reality, occultation measurements[7,16,17] provide bounds on the shape of the planet (radius versus latitude), and as shown below this allows the rotation period to be further constrained[8,18,19].

The best measurement uncertainty of Saturn's radii from radio and stellar occultation is ~6 km (ref. 17), although the actual uncertainty could be larger owing to the unknown contribution of the atmospheric dynamics[6] to the measured shape[20]. We therefore explore a range of uncertainty in mean radius between 6 km and 80 km. The results for this case are shown in Fig. 2b where P_{calc} and its standard deviation versus the uncertainty in observed radius R_{obs} are shown. The standard deviation (blue shading) of P_{calc} decreases with decreasing uncertainty in the radius. For an uncertainty of 6 km in Saturn's mean radius we derive a rotation period of 10 h 34 min 22 s ± 3.5 min. It is important to note that the derived period when using only the gravitational field is larger than P_{voy} while the derived period with the shape constraint is faster than P_{voy} (see Methods and Fig. 3 in Extended Data). It is clear that the parameter space of possible solutions narrows when the constraint of Saturn's measured mean radius is included. Yet, geopotential variations caused by atmospheric dynamics affect the shape of the planet, and therefore care should be taken when considering these measurements. By taking this hierarchal approach we are able to isolate the uncertainty given estimates of shape and internal structure separately. More conservative uncertainties in radius (tens of kilometres) yield longer rotation periods, thus giving solutions closer to the Voyager rotation period (see Fig. 2b).

The uncertainty in P_{calc} can be decreased even further if we also limit the range of the figure functions, that is, the density profile (Fig. 2c). Limiting the figure functions to within a range implied by interior structure models[21,22] (see Methods), the derived period is found to be 10 h 32 min 45 s ± 46 s. This rotation period is in agreement with previous calculations that derived Saturn's rotation period by using a fit to Saturn's measured shape[8]. The fact that the rotation period is shorter than the Voyager rotation period also implies that the latitudinal wind structure is more symmetrical, thus containing both easterly and westerly jets as on Jupiter[9,23]. Although the smallest possible uncertainty in rotation period is desirable, there is a clear advantage in not specifying constraints on the density profile, and keeping the method as general as possible.

Unlike Saturn's, the rotation period of Jupiter is well determined owing to its tilted magnetic field. Jupiter's measured rotation period (system III) is 9 h 55 min 29.69 s (refs 24, 25). To verify the robustness of our results we apply this method also for Jupiter (Fig. 3). When only the gravitational moments are used as constraints (Fig. 3a), as for Saturn, the uncertainty in the calculated rotation period is much smaller than the allowed range, and converges towards Jupiter's rotation period. Figure 3b shows the sensitivity of the derived period, when the uncertainty in period is ±0.5 h around the measured value, for a range of possible mean radii. As for Saturn, the standard deviation of P_{calc} decreases with decreasing ΔR. When the variation in R_{obs} is taken to be 6 km, a rotation period of 9 h 56 min 6 s ± 1.5 min is derived, consistent with Jupiter's measured rotation period. When we also add constraints on the figure functions, the derived rotation period becomes 9 h 55 min 57 s ± 40 s, showing that our method reproduces Jupiter's rotation period successfully.

The determination of Saturn's J_{2n} is expected to improve substantially following Cassini's end-of-mission proximal orbits. To test whether a more accurate determination of Saturn's gravitational field will allow us to better constrain its rotation period, we repeat the optimization with the expected new uncertainty on the gravitational moments ($\Delta J_{2n} \approx 10^{-9}$)[26] around the currently measured values. The solution making no assumptions on the density profile is shown in Fig. 4a. Since Jupiter's gravitational field will be more tightly determined by the Juno spacecraft[26,27] we do a similar analysis for Jupiter (Fig. 4b). While for Jupiter the calculated rotation period remains the same with the more accurate gravitational field, for Saturn the calculated uncertainty of

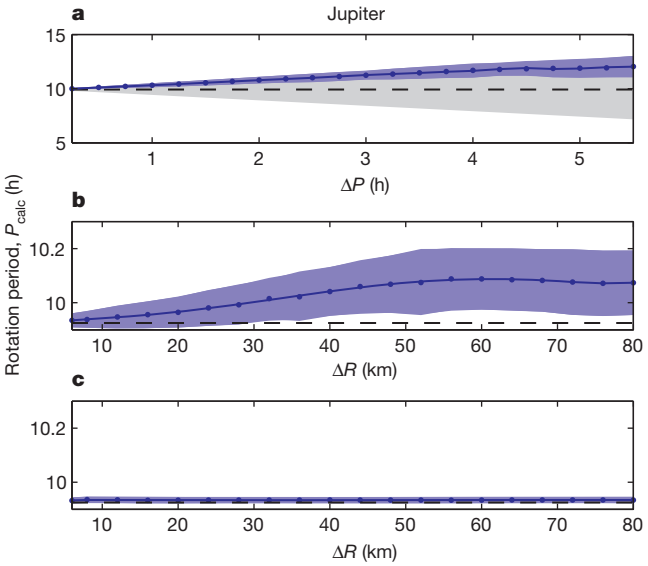

Figure 3 | Solutions for Jupiter's rotation period. **a**, The calculated period P_{calc} (blue dots) and its 1σ standard deviation (blue shading) for a large range of cases for which the assumed possible range in rotation period varies between 0.25 h and 5.5 h, that is, between ~5 h and 15 h (grey shading) around Jupiter's measured period (black-dashed line). **b**, P_{calc} and its 1σ standard deviation (blue shading) using $\Delta P = 0.5$ h versus the uncertainty in the assumed uncertainty in Jupiter's observed mean radius R_{obs}. **c**, As for **b** but when the figure functions are also constrained.

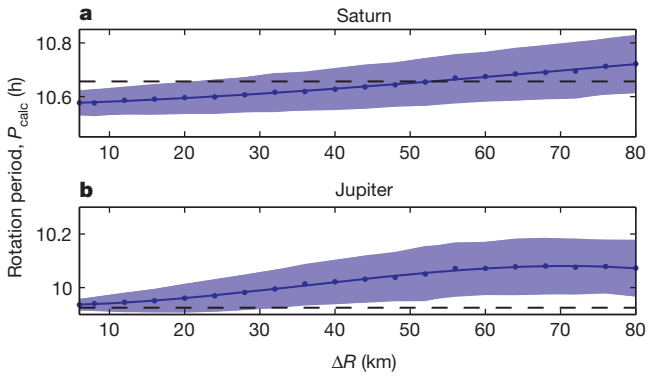

Figure 4 | Solutions for the rotation periods of Saturn and Jupiter when assuming improved gravity data. **a**, Saturn; **b**, Jupiter. Shown are P_{calc} and its 1σ standard deviation (blue shading) when setting $\Delta J_{2n} = 10^{-9}$ and $\Delta P = 0.5$ h. The calculated period is given versus the assumed uncertainty in the observed mean radius R_{obs}.

P_{calc} decreases by ~15%. We therefore conclude that the future measurements by Cassini could be important to further constrain Saturn's rotation period.

Online Content Methods, along with any additional Extended Data display items and Source Data, are available in the online version of the paper; references unique to these sections appear only in the online paper.

Received 2 September 2014; accepted 2 February 2015.
Published online 25 March 2015.

1. Sterenborg, M. G. & Bloxham, J. Can Cassini magnetic field measurements be used to find the rotation period of Saturn's interior? *Geophys. Res. Lett.* **37,** 11201 (2010).
2. Smith, B. A. *et al.* A new look at the Saturn system: the Voyager 2 images. *Science* **215,** 504–537 (1982).
3. Gurnett, D. A. *et al.* Radio and plasma wave observations at Saturn from Cassini's approach and first orbit. *Science* **307,** 1255–1259 (2005).
4. Gurnett, D. A. *et al.* The variable rotation period of the inner region of Saturn's plasma disk. *Science* **316,** 442–445 (2007).
5. Giampieri, G., Dougherty, M. K., Smith, E. J. & Russell, C. T. A regular period for Saturn's magnetic field that may track its internal rotation. *Nature* **441,** 62–64 (2006).
6. Sanchez-Lavega, A., Rojas, J. F. & Sada, P. V. Saturn's zonal winds at cloud level. *Icarus* **147,** 405–420 (2000).
7. Lindal, G. F., Sweetnam, D. N. & Eshleman, V. R. The atmosphere of Saturn—an analysis of the Voyager radio occultation measurements. *Astrophys. J.* **90,** 1136–1146 (1985).
8. Anderson, J. D. & Schubert, G. Saturn's gravitational field, internal rotation, and interior structure. *Science* **317,** 1384–1387 (2007).
9. Read, P. L., Dowling, T. E. & Schubert, G. Saturn's rotation period from its atmospheric planetary-wave configuration. *Nature* **460,** 608–610 (2009).
10. Zharkov, V. N. & Trubitsyn, V. P. *Physics of Planetary Interiors* 388 (Pachart Publishing House, 1978).
11. Hubbard, W. B. *Planetary Interiors* 1–343 (Van Nostrand Reinhold, 1984).
12. Schubert, G., Anderson, J., Zhang, K., Kong, D. & Helled, R. Shapes and gravitational fields of rotating two-layer Maclaurin ellipsoids: application to planets and satellites. *Phys. Earth Planet. Inter.* **187,** 364–379 (2011).
13. Kaspi, Y., Showman, A. P., Hubbard, W. B., Aharonson, O. & Helled, R. Atmospheric confinement of jet streams on Uranus and Neptune. *Nature* **497,** 344–347 (2013).
14. Jacobson, R. A. *JUP230 Orbit Solutions* http://ssd.jpl.nasa.gov/ (2003).
15. Jacobson, R. A. *et al.* The gravity field of the Saturnian system from satellite observations and spacecraft tracking data. *Astrophys. J.* **132,** 2520–2526 (2006).
16. Hubbard, W. B. *et al.* Structure of Saturn's mesosphere from the 28 SGR occultations. *Icarus* **130,** 404–425 (1997).
17. Flasar, F., Schinder, P. J., French, R. G., Marouf, E. A. & Kliore, A. J. Saturn's shape from Cassini radio occultations. *AGU Fall Meet. Abstr.* B8 (2013).
18. Helled, R., Schubert, G. & Anderson, J. D. Jupiter and Saturn rotation periods. *Planet. Space Sci.* **57,** 1467–1473 (2009).
19. Helled, R. Jupiter's occultation radii: implications for its internal dynamics. *Geophys. Res. Lett.* **38,** 8204 (2011).
20. Helled, R. & Guillot, T. Interior models of Saturn: including the uncertainties in shape and rotation. *Astrophys. J.* **767,** 113 (2013).
21. Guillot, T. The interiors of giant planets: Models and outstanding questions. *Annu. Rev. Earth Planet. Sci.* **33,** 493–530 (2005).
22. Fortney, J. J. & Nettelmann, N. The interior structure, composition, and evolution of giant planets. *Space Sci. Rev.* **152,** 423–447 (2010).
23. Dowling, T. E. Saturn's longitude: rise of the second branch of shear-stability theory and fall of the first. *Int. J. Mod. Phys. D* **23,** 1430006–86 (2014).
24. Higgins, C. A., Carr, T. D. & Reyes, F. A new determination of Jupiter's radio rotation period. *Geophys. Res. Lett.* **23,** 2653–2656 (1996).
25. Porco, C. C. *et al.* Cassini imaging of Jupiter's atmosphere, satellites and rings. *Science* **299,** 1541–1547 (2003).
26. less, L., Finocchiaro, S. & Racioppa, P. The determination of Jupiter and Saturn gravity fields from radio tracking of the Juno and Cassini spacecraft. *AGU Fall Meet. Abstr.* B1 (2013).
27. Finocchiaro, S. & less, L. in *Spaceflight Mechanics 2010* Vol. 136, 1417–1426 (American Astronautical Society, 2010).

Acknowledgements We thank G. Schubert, M. Podolak, J. Anderson, L. Bary-Soroker, and the Juno science team for discussions and suggestions. We acknowledge support from the Israel Space Agency under grants 3-11485 (R.H.) and 3-11481 (Y.K.).

Author Contributions R.H. led the research. R.H. and Y.K. initiated the research and wrote the paper. E.G. designed the optimization approach and executed all the calculations. R.H. computed interior models and defined the parameter space for the figure functions. All authors contributed to the analysis and interpretation of the results.

Author Information Reprints and permissions information is available at www.nature.com/reprints. The authors declare no competing financial interests. Readers are welcome to comment on the online version of the paper. Correspondence and requests for materials should be addressed to R.H. (rhelled@post.tau.ac.il).

METHODS

The theory of figures. The theory of figures was first introduced by Clairaut[28], who derived an integro-differential equation for calculating the oblateness of a rotating planet in hydrostatic equilibrium with a non-uniform density profile. The method was further developed by Zharkov and Trubitsyn[10], who presented a theoretical description to connect the density profile of a hydrostatic planet with its gravitational moments J_{2n}, extending the theory to an arbitrary order. The basic idea of the method is that the density profile of a rotating planet in hydrostatic equilibrium can be derived by defining the layers as level surfaces, that is, surfaces of a constant potential (called the effective potential) that is set to be the sum of the gravitational potential and the centrifugal potential[10,11]:

$$U=\frac{GM}{r}\left(1-\sum_{n=1}^{\infty}\left(\frac{a}{r}\right)^{2n}J_{2n}P_{2n}(\cos\theta)\right)+\frac{1}{2}\omega^2r^2\sin^2\theta \quad (1)$$

where r is the radial distance, a is the equatorial radius of the geoid, GM is its mass multiplied by the gravitational constant, θ is the colatitude, and ω is the angular velocity given by $2\pi/P$, with P being the rotation period.

The internal density profile and the gravitational moments are linked through the smallness parameter $m=\omega^2R^3/GM$, where R is the mean radius of the planet. The gravitational moments can be expanded as a function of m by:

$$J_2=ma_{2,1}+m^2a_{2,2}+m^3a_{2,3} \quad (2a)$$

$$J_4=m^2a_{4,2}+m^3a_{4,3} \quad (2b)$$

$$J_6=m^3a_{6,3} \quad (2c)$$

where $a_{2n,k}$ are the expansion coefficients in smallness parameter. As $J_2\gg J_4\gg J_6$ higher-order coefficients correspond to a higher-order expansion in m. The gravitational moments J_{2n} are determined from the combination of the internal density distribution as well as the rotation period. As a result, unless the density profile of Saturn (or any other giant planet) is perfectly known there is no simple way to derive the rotation period and vice versa.

For the investigation of planetary figures, the equation for level surfaces can be written in the form of a spheroid that is a generalized rotating ellipsoid. Then, the planetary radius r at every latitude can be expressed as a function of the polar angle θ (colatitude), and the flattening parameters f, k and h by[10,12]:

$$r(\theta)=a\left[1-f\cos^2\theta-\left(\frac{3}{8}f^2+k\right)\sin^2 2\theta+\frac{1}{4}\left(\frac{1}{2}f^3+h\right)\left(1-5\sin^2\theta\right)\sin^2 2\theta\right] \quad (3)$$

where $f=(a-b)/a$ is the flattening (with b being the polar radius), and k and h are the second-order and third-order corrections, respectively[10]. While f is strictly the flattening of the object, k and h represent the departure of the level-surface from a precise rotating ellipsoid to second and third order in smallness parameter, and their values are expected to be much smaller than f.

To third order, the three flattening parameters f, k, h at the planetary surface (the effective potential surface) can be written as a sum of figure functions defined by[12]:

$$f=mF_1+m^2F_2+m^3F_3 \quad (4a)$$

$$k=m^2K_2+m^3K_3 \quad (4b)$$

$$h=m^3H_3 \quad (4c)$$

Finally, using the relation between the first three even gravitational moments and the figure functions for a density profile that is represented by a 6th-order polynomial[8,12,13] and by applying the theory of figures as a set of differential equations, the gravitational moments and the figure functions can be related as power series in the small rotational parameter m (see equation (72) in ref. 12). Since only J_2, J_4 and J_6 are currently known for Saturn (and Jupiter) we expand only up to third order in m. Although higher-order harmonics are not expected to be zero, the corrections will be $O(m^4)$ and therefore their contribution will be small.

The optimization method. Since the flattening parameters (and figure functions) depend on the density distribution, which is unknown, we take a general approach that is designed to relate the planetary rotation period to its gravitational field without putting tight constraints on the internal structure. We therefore develop an optimization method that searches for the solutions that reproduce Saturn's measured gravitational field within the widest possible pre-defined parameter space. The figure functions (F, H, K) are allowed to vary over their widest possible physical range, and the smallness parameter m is allowed to vary within a range that reflects the uncertainty in the rotation period P. A solution for these parameters is sought while meeting the requirement that Saturn's measured physical properties are reproduced.

First, an optimization function is defined as the sum of the normalized absolute differences between the observed moments and the calculated moments and is given by:

$$Y=\sum\left(\frac{\left|J_2-J_2^{\rm obs}\right|}{\left|\Delta J_2^{\rm obs}\right|}+\frac{\left|J_4-J_4^{\rm obs}\right|}{\left|\Delta J_4^{\rm obs}\right|}+\frac{\left|J_6-J_6^{\rm obs}\right|}{\left|\Delta J_6^{\rm obs}\right|}\right) \quad (5)$$

where J_2, J_4 and J_6 are the gravitational moments calculated using equations (2a–c), $J_2^{\rm obs}$, $J_4^{\rm obs}$ and $J_6^{\rm obs}$ are the measured gravitational moments, and $\Delta J_2^{\rm obs}$, $\Delta J_4^{\rm obs}$ and $\Delta J_6^{\rm obs}$ are the uncertainties on the measured gravitational moments[14,15]. Since the observations include only the first three even harmonics everything is calculated to third order, but the method can be modified to include higher-order terms. The data that are used by the model are summarized in Extended Data Table 1.

Next, we minimize the optimization function Y with respect to the control variables F_1, F_2, F_3, K_2, K_3, H_3 and m, that is, the figure functions, and the smallness parameter. Starting from an arbitrary initial guess for each of the seven control variables (within the predefined limits), a solution is sought such that the optimization function reaches a minimum. Several nonlinear constraints are imposed while searching for the solution. First, we require that the difference between each calculated and the measured gravitational moments must be smaller than the uncertainty of the measurement error, that is, $\left|J_2-J_2^{\rm obs}\right|-\left|\Delta J_2^{\rm obs}\right|<0$, $\left|J_4-J_4^{\rm obs}\right|-\left|\Delta J_4^{\rm obs}\right|<0$, and $\left|J_6-J_6^{\rm obs}\right|-\left|\Delta J_6^{\rm obs}\right|<0$. Note that this requirement is additional to the minimization of Y since we ask that not only the overall difference between the observed and calculated gravitational moments is minimized, but that individually, each of the calculated moments stays within the uncertainty of its observed counterpart.

The parameter f is the planetary flattening; as a result, f must be a small positive number (for Saturn $f\approx 0.1$). The second- and third-order corrections, k and h, are substantially smaller than f, but could be either positive or negative. Thus, in order to keep our calculation as general as possible we allow the three flattening parameters to vary between their maximum physical values, -1 and 1. In Extended Data Fig. 1 we show the calculated values for f, h, k for Saturn for the case in which the figure functions are not constrained and ΔR is taken to be 50 km. f is found to be of the order of 0.1, consistent with the measured flattening of Saturn[7,20], while the second-order and third-order corrections are found to be of the order of 10^{-3}. As F_1 is the first-order expansion for f, we have $f-F_1m=O(m^2)$, meaning that for Saturn $|F_1|<1$. Similarly expanding recursively the other coefficients of f, and also those of k and h, implies that all figure functions are bound between -1 and 1. To keep our calculation as general as possible we allow all the figure functions to vary between -1 and 1. The solution though, which must also fit the gravitational field, constrains the flattening parameters and figure functions to a much narrower range. The solution is derived by using a numerical algorithm that is designed to solve constrained nonlinear multivariable functions. We use a sequential quadratic method that formulates the above nonlinear constraints as Lagrange multipliers[29]. The optimization is completed once the tolerance values for the function (10^{-3}) and the constraints (10^{-12}) are met.

A single optimization would be sufficient if the problem was well defined. In such a case, there would have been a unique solution that is independent of the initial guess. However, since in our case there are only three equations (equations (2a–c)) and seven unknowns (six figure functions and the smallness parameter), the problem is inherently ill-defined and therefore has no unique solution. Nevertheless, we can still reach a solution using a 'statistical' approach in which we repeat the optimization process enough times to achieve a statistically stable solution. In each case, the initial guess of the various parameters is chosen randomly within the defined bounds of each parameter. A statistical significance is reached when we repeat the optimization 2,000 times (verified with 10^4 optimizations). We can then use the solutions from the 2,000 optimizations to compute the mean value and its standard deviation for each variable. An example for a specific case is given in Extended Data Fig. 2, where the solutions for the gravitational moments (Extended Data Fig. 2a–c) are distributed around the mean value, and the distribution of the solutions for the figure functions (Extended Data Fig. 2d–j) has a large range. From each such experiment we eventually calculate two numbers: the mean rotation period $P_{\rm calc}$ and its standard deviation.

Expected improvements from Cassini's proximal orbits. Another objective of this research is to determine whether the improved gravity measurements of the low-order gravitational moments (J_2, J_4, J_6) by the Cassini's proximal orbits mission can be used to better constrain Saturn's rotation period. The data are not yet available, but are expected to be within the current uncertainty, so all we can do at present is estimate the rotation period and its standard deviation when the uncertainty on the gravitational moments (ΔJ_{2n}) is of the order of 10^{-9} while using the currently known values of J_2, J_4, and J_6. The result for this exercise is presented in Fig. 4. It is found that for Saturn this yields a 15% improvement in the derived

standard deviation of its rotation period. However, it is important to remember that the true values of the gravitational moments can be any value within the current uncertainty. We find that the order of magnitude of the standard deviation is not very sensitive to the actual value of J_{2n} but is more affected by the allowed uncertainty (that is, ΔJ_{2n}); we can therefore conclude that the Cassini proximal orbit measurement is useful to further constrain Saturn's rotation period.

Accounting for the planetary shape. Our optimization method can include additional constraints. Since the planetary shape could be used to constrain the rotation period[18,20], we also run cases in which we account for Saturn's shape (see equation (4)). Then the optimization includes the constraint that the calculated mean radius R should be consistent with the mean radius that is inferred from measurements. Thus, the calculated mean radius R_{calc} should be less than a specified uncertainty, that is:

$$|R_{calc} - R_{obs}| - |\Delta R| < 0 \quad (6)$$

where R_{obs} is the mean radius estimated from measurements of the planetary shape, and ΔR is the uncertainty associated with the measured radius. In the standard case we set this uncertainty to be 40 km, which is large compared to the measured uncertainty in Saturn's shape[7]. This provides a fourth equation to our optimization method and allows a considerable reduction in the rotation period uncertainty (Figs 2b and 3b).

Although Saturn's measured shape (radius as a function of latitude) is well determined from occultation measurements[7,16], one should note that there is a difference between the measurement uncertainty (estimated to be ~6 km; refs 7, 17) and the actual uncertainty (of the order of a few tens of kilometres[20]). The actual uncertainty is relatively large because the planet's measured shape is also affected by atmospheric winds, which distort the hydrostatic shape. The equatorial region of Saturn is affected by the large equatorial winds, and indeed the dynamical heights of the equator are found to be ~120 km (refs 7, 8, 16 and 20). On the other hand, the polar region is less affected by winds, and therefore the polar radii better reflect Saturn's hydrostatic shape. There are, however, no available occultation measurements of Saturn's polar regions. In addition, Saturn's north–south asymmetry in wind structure introduces an additional uncertainty in determining its shape. As a result, a more conservative uncertainty in Saturn's mean radius is estimated to be ~40 km (ref. 20).

Interestingly, the solution for the rotation period for the case without the shape constraint does not necessarily contain the solution when the constraint on the shape is included. This is caused by the fact that taking into account only the gravitational moments, for Saturn, leads to a solution with relatively long rotation periods, while the measured shape pushes to shorter rotation periods. This effect is illustrated in Extended Data Fig. 3 where the solutions for the rotation period are shown in the phase-space of the constraints for ΔP and ΔR. When there is no constraint on the shape, and ΔP is large (upper-right, red region), the solution converges to a relatively long rotation period; as ΔP decreases, solutions with shorter rotation periods can be found (upper-left, blue region, see also Fig. 2a). When the constraint on the shape is included, even when the range of the rotation period is large (bottom-right, blue region), the solution converges into a short rotation period. The dashed line shows the transition between the regime where the constraint on the period (above the dashed line) to the regime where the constraint on the shape is more important. For the physical region we are interested in, as the constraint on the shape is increased (as $\Delta\bar{R}$ decreases), it becomes more dominant than the constraint on the rotation period, leading to a shorter rotation period outside the range of the solution without the shape constraint.

Constraining the figure functions. We also present results for cases in which the figure functions are constrained as well (Figs 2c and 3c for Saturn and Jupiter, respectively). In these cases, the figure functions are limited to a range that is determined from realistic interior models[21,22]. To put limits on their values, we run two limiting interior models for both Saturn and Jupiter and derive the values of the figure functions. The first case is one of a massive core, for which we assume a constant-density core with a density of $\sim 1.5 \times 10^4\,\mathrm{kg\,m^{-3}}$, reaching 20% of the planet's radius. In the second case, the density is continuous with no core and is represented by a 6th-order polynomial. For this case, the first-degree term of the polynomial is missing so that the derivative of the density goes to zero at the centre. Another constraint sets this value to zero at the core-envelope boundary for models with cores. We then use the derived values of the figure functions for each case to limit the values of the variables F_1, F_2, F_3, K_2, K_3 and H_3.

The figure functions we derive for the massive core and continuous density profile cases for Saturn and Jupiter are summarized in Extended Data Table 2. The density profiles for Saturn (top) and Jupiter (bottom) are shown in Extended Data Fig. 4. The values of the figure functions for interior models intermediate to these extreme cases all lie within the values of the extreme cases, implying that we have taken an exclusive set of values. To make sure that we account for a relatively large range of possible interior models, even within this fairly constrained case, we allow the figure function values to vary around the average value between the two models by a factor of two of the difference. The results (for Saturn) are shown in Extended Data Fig. 5. It is clear that in this case, due to the limitation on the figure functions, the parameter space of possible solutions is smaller, allowing a more accurate determination of P_{calc}. This range still accounts for a large variation in Saturn's density profile. While there is an improvement in the determination of P_{calc} when the shape and figure functions are tightly constrained, there is also a clear advantage in keeping the method as general as possible. The inferred result is then not associated with a specific interior model and/or does not rely on shape measurements. Our method is therefore also useful for estimating the rotation period of giant planets with less accurate determinations of their physical properties. For the icy planets, Uranus and Neptune, only J_2 and J_4 are currently known, yet a simplified version of this optimization (to second order) can be applied and gives rotation periods within 2% of the Voyager radio periods, allowing an independent method for estimating their rotation periods from their gravitational moments. Furthermore, our method could also be applied to derive the rotation periods of exoplanets for which the gravitational moments can be estimated[30,31].

Code availability. The optimization code (written in Matlab) that was used to calculate the rotation period and its standard deviation is available at http://www.weizmann.ac.il/EPS/People/Galanti/research.

28. Clairaut, A. C. *Traite de la Figure de la Terre, tiree des Principes de l'Hydrostatique* (Paris Courcier, 1743).
29. Nocedal, J. & Wright, S. J. *Conjugate Gradient Methods* 102–120 (Springer, 2006).
30. Carter, J. A. & Winn, J. N. Empirical constraints on the oblateness of an exoplanet. *Astrophys. J.* **709,** 1219–1229 (2010).
31. Kramm, U., Nettelmann, N., Fortney, J. J., Neuhäuser, R. & Redmer, R. Constraining the interior of extrasolar giant planets with the tidal Love number k_2 using the example of HAT-P-13b. *Astron. Astrophys.* **538,** A146 (2012).

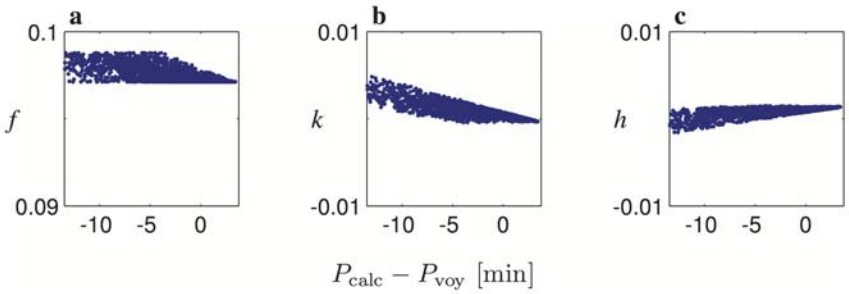

Extended Data Figure 1 | The flattening parameters calculated by the model without constraining the figure functions. Shown are f, k, h for Saturn with $\Delta R = 50$ km.

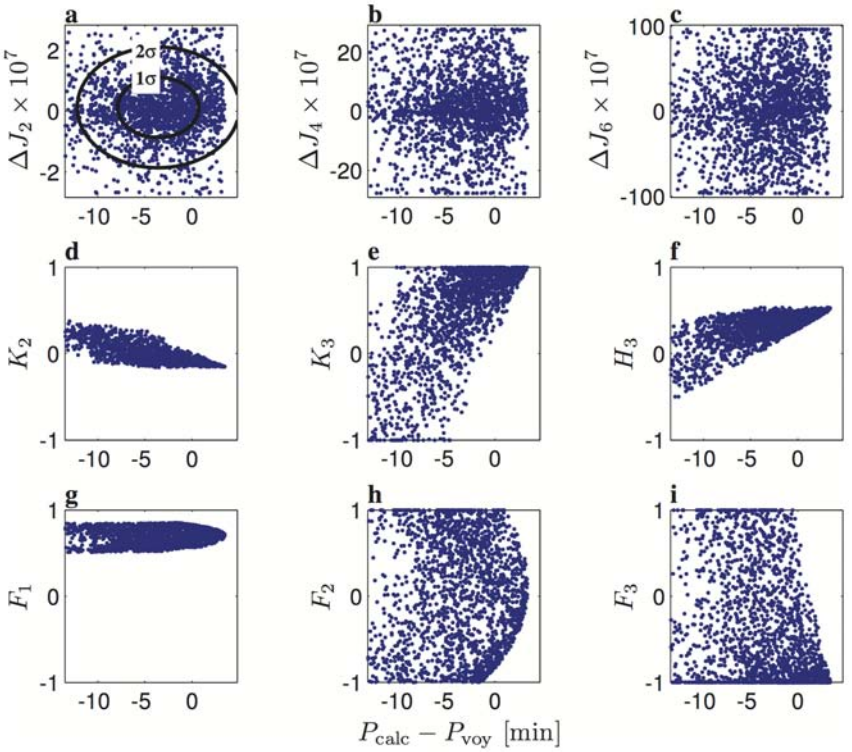

Extended Data Figure 2 | An example of our statistical optimization model for deriving the rotation period. The results are shown for a case for which the range of allowed rotation period is between 10 h 24 min and 10 h 54 min. The solution is based on a combination of 2,000 individual sub-cases, each of them representing a case with specific random initial conditions within the defined parameter space. **a**–**c**, A scatter plot (similar to Fig. 1a) of the distribution of solutions on the plane of the calculated rotation period P_{calc} minus P_{voy} versus each of ΔJ_2, ΔJ_4 and ΔJ_6. Each blue dot represents one sub-case converged solution. In **a** the inner and outer black circles show the first and second standard deviations, respectively. **d**–**j**, The distribution of solutions for the figure functions K_2, K_3, H_3, F_1, F_2 and F_3, respectively.

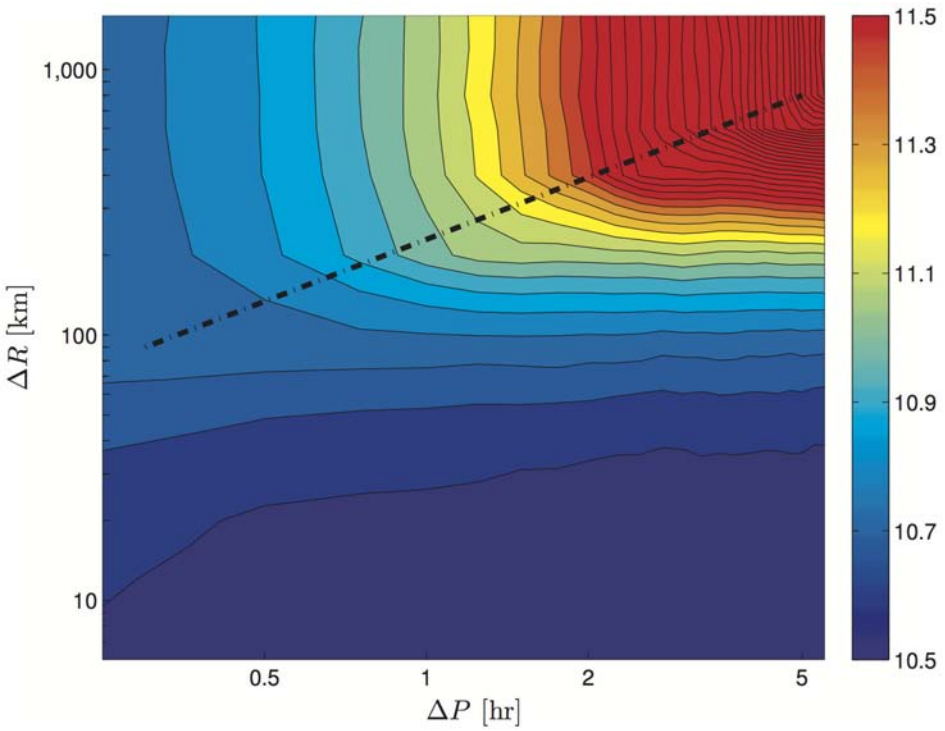

Extended Data Figure 3 | Saturn's calculated rotation period versus the uncertainty in the assumed rotation period and radius. P_{calc} shown (colour scale) as a function of ΔP (h) and ΔR (km). The dashed line presents the transition from the regime where the constraint on the rotation period (above the dashed line) to the regime where the constraint on the shape is more dominant.

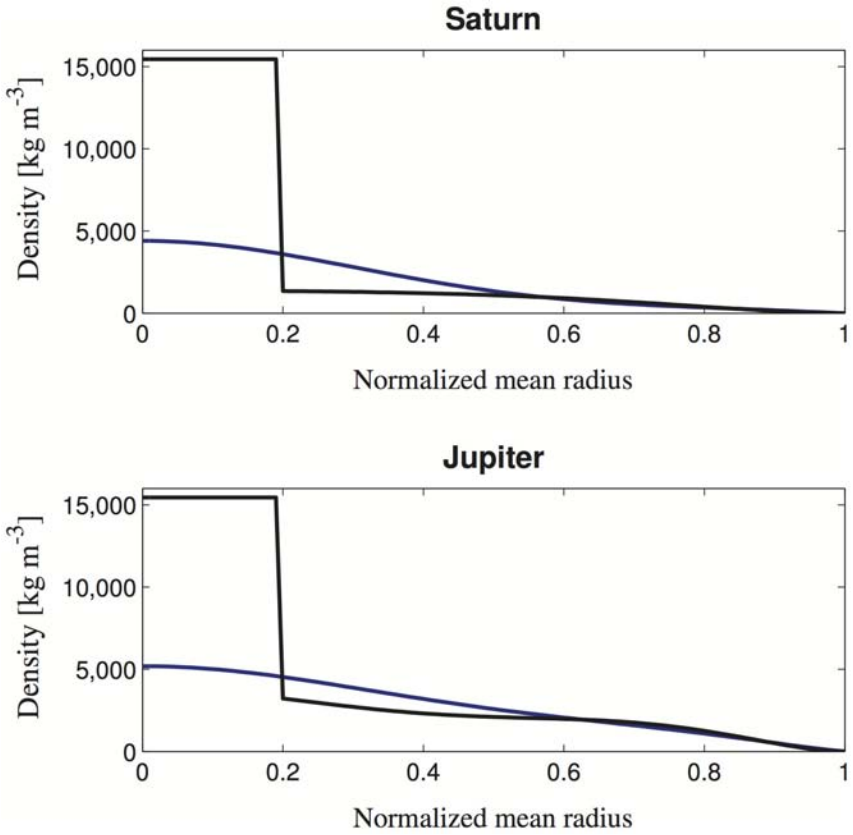

Extended Data Figure 4 | Radial density profiles for two different interior models for Saturn (top) and Jupiter (bottom). The black curves correspond to models with very large cores and the blue curves are no-core models in which the density profile is represented by 6th-order polynomials. For the massive-core case we assume a constant core density of $\sim 1.5 \times 10^4\,\mathrm{kg\,m^{-3}}$, reaching 20% of the planet's radius. The density profiles are constrained to match the planetary mass, J_2, J_4, J_6, mean radius, and the atmospheric density and its derivative at 1 bar (see details in refs 8, 13 and 18). We then use the difference in the values of the figure functions in the two limiting cases to limit their values.

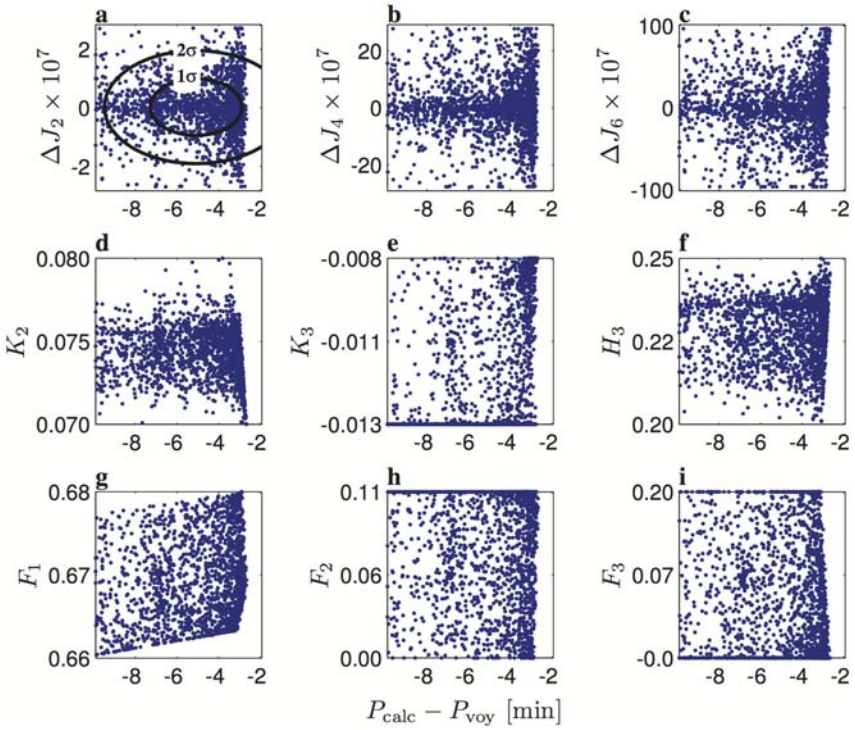

Extended Data Figure 5 | The calculated flattening parameters when the figure functions are limited by interior models. **a**–**c**, A scatter plot (similar to Fig. 1a) of the distribution of solutions on the plane of the calculated rotation period $P_{\rm calc}$ minus $P_{\rm voy}$ versus ΔJ_2, ΔJ_4 and ΔJ_6, respectively. Each blue dot represents one sub-case converged solution. The calculated mean radius was set to be within 20 km of Saturn's observed mean radius. In **a** the inner and outer black circles show the first and second standard deviations, respectively. **d**–**j**, The distribution of solutions for the figure functions K_2, K_3, H_3, F_1, F_2 and F_3, respectively.

Extended Data Table 1 | The physical properties of Saturn and Jupiter used in the analysis

	Saturn	Jupiter
Mass (10^{24} kg)	568.36	1,898.3
Rotation Period (System III)	10hr 39m 24s	9hr 55m 29s
Mean Radius (km)	58,232	69,911
J_2 (10^{-6})	$16,290.71 \pm 0.27$	$14,696.43 \pm 0.21$
J_4 (10^{-6})	-935.83 ± 2.77	-587.14 ± 1.68
J_6 (10^{-6})	86.14 ± 9.64	34.25 ± 5.22

Data are taken from http://ssd.jpl.nasa.gov/?gravity_fields_op (JUP 230). The gravitational moments correspond to a reference equatorial radius of 60,330 km and 71,492 km for Saturn and Jupiter, respectively.

Extended Data Table 2 | The calculated figure functions based on interior models of Saturn and Jupiter

	Saturn - Massive Core	Saturn - No Core
F_1	0.66357	0.67720
F_2	0.07501	0.04743
F_3	0.043517	0.10790
K_2	0.22691	0.07535
K_3	-0.01039	-0.01174
H_3	0.10074	0.23489
	Jupiter - Massive Core	**Jupiter - No Core**
F_1	0.77014	0.76965
F_2	0.08512	0.08499
F_3	0.14874	0.15137
K_2	0.05868	0.05861
K_3	-0.00705	-0.01068
H_3	0.19885	0.20570

The values of the figure functions are derived for the two limiting cases of massive core and no-core (continuous density profile) for Saturn and Jupiter.